Int J Biochem Mol Biol 2012;3(1):58-69
www.ijbmb.org /ISSN:2152-4114/IJBMB1201005

Original Article

Crystal structure of peptidyl-tRNA hydrolase from mycobacterium smegmatis reveals novel features related to enzyme dynamics

Ashok Kumar[1], Nagendra Singh[2,*], Rahul Yadav[1], Ramasamy P. Kumar[2], Sujata Sharma[2], Ashish Arora[1], T. P. Singh[2]

*[1]Molecular and Structural Biology Division, CSIR-Central Drug Research Institute, Lucknow, India; [2]Department of Biophysics, All India Institute of Medical Sciences, New Delhi, India. *Current address: Gautum Budha University, NOIDA, India*

Received January 15, 2012; accepted February 8, 2012; Epub February 15, 2012; Published March 15, 2012

Abstract: Peptidyl- tRNA hydrolase from Mycobacterium smegmatis is a single domain 21 kDa protein involved in the hydrolysis of prematurely produced peptidyl-tRNAs to ensure the viability of cells in bacteria, thus making it a potentially important drug target. In order to aid the development of potent drugs for controlling bacterial infections, the three-dimensional structure of peptidyl-tRNA hydrolase from Mycobacterium smegmatis has been determined. The protein adopts a compact α/β globular fold with a twisted β-sheet surrounded by α-helices. The functionally important C-terminal stretch has been unambiguously modeled for the first time in the unliganded structure of peptidyl-tRNA hydrolase. The segment, Gly138 - Val150 is mobile because it lacks significant interactions with the rest of the protein molecule. This conformational flexibility is reflected through different values of distances between a reference atom Ala147 C^{α} of the segment Gly138 - Val150 to Gly114 C^{α} from another segment from opposite side of the substrate binding channel in Mycobacterium smegmatis (7.8 Å), Mycobacterium tuberculosis (9.5 Å) and Escherichia coli (11.8 Å). Similarly, the conformation of loop Gly109 - Gly117 with respect to another loop Asp95 - Asp100 also shows variability of the substrate binding cleft as the distance between Asp98 $O^{\delta 2}$ to Gly113 C^{α} in Mycobacterium smegmatis is 4.5 Å while the corresponding distances in Mycobacterium tuberculosis and Escherichia coli are 3.1 Å and 6.7 Å respectively. The hydrogen bonded interactions between Asn116, His22 and Asp95 indicate a stereochemically favorable arrangement of these residues for catalytic action.

Keywords: Peptidyl-tRNA hydrolase, cloning, crystal structure, mycobacterium smegmatis, c-terminus, protein expression

Introduction

Peptidyl-tRNA hydrolase (Pth, EC. 3.1.1.29), an esterase, catalyzes the release of tRNA from the prematurely terminated translation product peptidyl-tRNA. It also plays a pivotal role in the functioning of several other key translational factors [1-5]. Pth was first identified in *Escherichia coli* [6-10] and yeast [11]. Subsequently, its homologues were also reported from other bacteria [12-15]. Although the crystal structures of peptidyl-tRNA hydrolase from *Escherichia coli* (EcPth) [13], *Mycobacterium tuberculosis* (MtPth) [14], *Sulfolobus solfataricus* (SuPth) [16], human (HuPth) [17] and *Pyrococcus horikoshii* OT3 (PhPth) [18] have been reported but the mode of binding and the mechanism of catalytic action are not yet fully understood. It may be mentioned here that bacteria contain a single Pth whereas eukaryotes possess several isoforms such as Pth1, Pth2 etc. In this regard, the bacterial enzymes are different from those of eukaryotes in lengths, amino acid sequences and structural folds and thus due to these differences the bacterial Pth are potentially attractive drug targets for developing new molecules against bacterial infections [13, 17]. Among the members of bacterial enzymes, MsPth has very low sequence homologies with Pyrococcus horikoshii (7%), human peptidyl-tRNA hydrolase (3%) and sulfolobus solfataricus peptidyl-tRNA hydrolase (2%). In contrast, MsPth has a similar chain length and significant sequence homologies

with peptidyl-tRNA hydrolases from other bacterial enzymes such as MtPth (80 %) and EcPth (38 %) whose crystal structures have been reported recently [13, 14] but enough information was not yet available about the stereochemical compatibility of the substrate binding site to the substrate, peptidyl-tRNAs with variable sizes of peptide moieties, the mode of binding of mixtures of peptidyl-tRNAs and the mechanism of catalytic action. The compact nature of the substrate binding site in the structure of the native enzyme and the mode of induction in the structure for accommodating the substrates for binding and catalysis are also not yet very clear. In the previous homologous structures of EcPth [13] and MtPth [14], it was mentioned that the interatomic distance between the nearest atoms of Asp98 and Gly113 as a possible indicator of the enzyme substrate binding interaction whether the ligand was bound to the enzyme or whether the enzyme was in the resting unbound state. These differences in the distances were also indicative of the conformational flexibility of the binding site. The conformational adaptability is particularly important in the case of peptidyl- tRNA hydrolases because the sizes of the peptide moieties of peptidyl-tRNAs vary considerably. Thus in order to deal with the mixed population of peptidyl-tRNAs of variable sizes, the enzyme must adopt variable conformations. For understanding the structural basis of the conformational inducibility in peptidyl - tRNA hydrolases and its relationship with enzyme action, we have determined the crystal structure of MsPth at 2.4 Å resolution. The structure has revealed the presence of several unique intramolecular interactions that determine the framework of MsPth and the lack of many interactions that allow segmental movements in the structure.

Materials and methods

Cloning, expression and protein purification

Genomic DNA from *Mycobacterium smegmatis* was prepared according to the method described by Kremer et al. [19]. The MsPth gene was PCR amplified using *Pyrococcus furiosus* DNA polymerase (fermentas) using 5′CAT GCC ATG GCC GAG CCG CTG CTG GTA GTG3′ and 5′ CCC AAG CTT CTA CCA GGC GTG GAC GGT GTT CTG 3′ as forward and reverse primers respectively. The PCR involved 30 cycles of initial denaturation at 368 K for 3 min, annealing at 340 K for 45 s and extension at 345 K for 1 min. The PCR product was digested with NcoI and HindIII and cloned into the same sites of the pETNH6 vector. The clone was verified by sequencing. The *E. coli* BL21 (λDE3) strain was used for expression of the recombinant MsPth protein. A single colony was inoculated in Luria-Bertani (LB) media supplemented with 100 mg/ml ampicillin and grown at 37°C. This overnight culture was used as a seed culture. The seed culture was reinoculated in fresh 1 liter LB medium and the required amount was inoculated with 1% of this culture and grown at 37°C with shaking (220 rpm) until the OD at 600 nm reached the value of 1.0. The culture was cooled down to 27°C and induced with 0.3 mM isopropyl-1-thio-β-D-galactopyranoside (IPTG) and grown for a further 13 h at 27°C with slower shaking (180 rpm). Cells were harvested by centrifugation at 4000 g for 10 min at 4°C. Approximately 1 g of the wet pellet was suspended in 15 - 20 ml of 50 mM Tris-HCl buffer containing 300 mM NaCl and 10 mM imidazole, pH 8.0 (lysis buffer) and stored at -80°C until further use. The cells were disrupted using cell disruption system at 22 KPSI (Constant Systems Ltd., England). The ruptured cells were centrifuged at 13000 g for 30 min at 4°C. The cleared lysate was applied to a Ni-NTA Superflow column (QIAGEN Gmbh, Germany) pre-equilibrated in lysis buffer and purified using stepwise washing with 30 mM lysis buffer followed by 300 mM imidazole in lysis buffer. A portion of each fraction was subjected to 15% sodium dodecyl sulphate - polyacrylamide gel electrophoresis (SDS-PAGE). The protein bands were visualized by staining the gel with Coomassie Brilliant Blue R250 (Sigma-Aldrich, St. Louis, Missouri, USA). The appropriate fractions were pooled and His-tag was removed by digestion with Tobacco Etch Virus (TEV) protease and the column was washed with the same buffer. MsPth did not bind to the column and was recovered from the flow-through. Appropriate fractions were pooled and concentrated using centricon of 5-kDa cut-off (Millipore Corporation, Billerica, Massachusetts, USA). The concentrated protein was purified using FPLC (Bio-rad, Berkeley, California, USA) with pre-packed superdex G-75, 10/300 column (GE Healthcare, Buckinghamshire, UK) in buffer containing 20 mM Tris-HCl, pH 8.0, 50 mM NaCl, 1.0 mM EDTA, and 5 mM β-mercaptoethanol. After purification the protein was concentrated to 6.0 mg/ml in a centricon of 5-kDa cut-off (Millipore India Pvt. Ltd, Bangalore, India). The protein concentration was esti-

mated using Bradford Reagent (Sigma-Aldrich, St. Louis, Missouri, USA) according to the supplier's protocol using bovine serum albumin (BSA) as standard.

Crystallization, structure determination and refinement of MsPth

FPLC purified samples of MsPth in the buffer containing 20 mM Tris-HCl, pH 7.5, 1 mM EDTA, 50 mM NaCl and 5 mM β-mercaptoethanol concentrated to 6 mg/ml. The reservoir solution was prepared with 30% (w/v) PEG-1500 and 10% isopropanol in 100 mM HEPES buffer, pH 6.5. 2 µl of the reservoir solution was added to the 5 µl of protein solution to make the sample drops of 7 µl. These drops were placed on the siliconized cover slips and equilibrated in a hanging drop vapour diffusion set up against the reservoir solution. X-ray intensity data were collected at 293K using a MAR research 345 mm dtb imaging plate scanner, mounted on a Rigaku RU-300 rotating anode X-ray generator operating at 50 kV and 100 mA. The structure of MsPth1 was solved using molecular replacement method with the program MOLREP [20] using coordinates of MtPth (PDB accession no: 2Z2I) as the search model [14]. The structure was refined using program CNS [21]. The protein chain was manually fitted into the electron density using programs COOT [22] and O [23]. The electron density in the Fourier $|(2Fo-Fc)|$ map contoured at 1.25 s was well defined for whole of C-terminal segment (residues 180 - 191). Based on the clear indications from the excellent electron densities in the Fourier $|(2Fo-Fc)|$ and difference Fourier $|(Fo-Fc)|$ maps, residues, Ser59, Cys67, Tyr68 and Ala156 were changed to Thr59, Ile67, Ser68, and Ser156 respectively. In the final stages of refinement, the positions of 141 water oxygen atoms were obtained from the difference $|(Fo-Fc)|$ Fourier maps. The final R_{cryst} and R_{free} (for 5% data) factors were 0.179 and 0.211 respectively.

Results

Quality of model

The refined final model of MsPth consists of 1428 protein atoms from all the 191 residues including the twelve C - terminal residues (180 - 191) which were not present in the previously reported homologous structure of MtPth [14]. The positions of 141 water oxygen atoms have also been determined accurately. The final crystallographic R-factor is 18.2% while the free R-factor for 5% reflections which were not included in the refinement is 22.1%. The molprobity score is 64 percentile [24]. As calculated using PROCHECK [25], 92.2% residues were found in the most favored regions of the Ramachandran map [26]. The refinement statistics has been included in **Table 1**.

Molecular structure

MsPth exists as a monomeric protein and adopts an α/β fold with seven β-strands, β1 (5 - 10), β2 (41 - 43), β3 (48 - 52), β4 (58 - 64), β5 (89 - 96), β6 (103 - 108) and β7 (130 - 136) and six α-helices, α1 (24 - 36), α2 (72 - 82), α3 (116 - 125), α4 (146 - 151), α5 (156 - 179), α6 (181 - 188). As seen from (**Figure 1A**), a twisted β-sheet is formed in the centre of the molecule by four parallel strands, β4, β1, β5 and β7. The β-sheet is flanked by two antiparallel β-strands, β2 and β3. The remaining β-strand, β6 is antiparallel to β-strand, β7 which is located next to the longest α-helix, α5. The centrally located β-sheet is surrounded by α-helices, α1, α2, α3, α5 and α6 in such a manner that α1, α5 and α6 are on one side while α2 and α3 are located on the opposite side. A short helix α4 is situated above the crevice as part of the mobile segment Gly138 - Val150 (**Figure 1A**). In fact, it can also be visualized that the seven β-strands are supported by two α-helices, α2 and α3 from below whereas α1, α5, α4 and α6 are placed above covering two sides completely. The putative substrate binding site in MsPth is indicated in red color (**Figure 1B**). The C-terminal segment consisting of residues Gly180 - Trp191 is well defined in the present structure except the last two residues Ala 190 and Trp191 for which electron density was weak though very characteristic to allow the unambiguous interpretation of these residues (**Figure 2A**). It is important to note that that the C-terminal segment forms several intramolecular contacts with the residues of neighboring β-strand β6 and α-helix α5 (**Figure 2A**). The important contacts of the C-terminal segment include hydrogen bonds, Gln185 $N^{\varepsilon 2}$ - - - O Leu106 = 2.8 Å, His189 $N^{\varepsilon 2}$ - - - N Leu106 = 3.2 Å and Gly180 N - - - O Leu176 = 2.9 Å. Apart from these interactions, the other stabilizing factor is provided by van der Waals contacts of Leu181 of the C-terminal segment with residues, Leu106, Leu108, His131, Leu175, Leu176, Ala184, and Gln185. The extensiveness of interactions involving Leu181 with neighboring residues indi-

Table 1. Data collection and refinement statistics.

Data Collection Statistics	
Space Group	$P2_12_12_1$
Unit Cell Dimensions	
A	45.0
B	59.0
C	62.1
Number of molecules in the unit cell	4
Vm (Å³/Da)	2.0
Resolution range (Å)	2 3 . 4 0 - 2.40
The highest resolution shell (Å)	2.50-2.40
Total number of measured reflections	34601
Number of unique reflections	6520
Completeness of data (%)	95 (98)
Rsym* (%)	11.5 (47.8)
I/s(I)	8.0 (2.5)
Refinement Statistics	
Rcryst+ (%)	18.2 (24.7)
$R_{free}$$ (5 % data)	22.1 (35.0)
Protein atoms	1428
Water oxygen atoms	141
R.m.s.d in bond lengths (Å)	0.008
R.m.s.d in bond angles (°)	1.6
R.m.s.d in torsion angles (°)	23.4
Mean B-Factors	
main chain atoms	28.2
side chain atoms	33.4
water atoms	47.8
all atoms	32.2
Ramachandran Plot	
Residues in the most allowed regions (%)	91.6
Residues in the additionally allowed regions (%)	8.4
Clash Score (percentile)[16]	**87**
Molprobity Score (percentile)[16]	**54**
PBD Accession Code	**3KJZ**

Values in parentheses are for the last shell. $*R_{sym}$ (I) = $\Sigma_{hkl} \Sigma_i | I_i (hkl) - I(hkl) | / \Sigma_{hkl} I_i (hkl)$; $^+R_{cryst} = \Sigma_{hkl} | F_{obs} - F_{calc} | / \Sigma_{hkl} F_{obs}$; $^\$R_{free} = \Sigma_{hkl} | F_{obs} - F_{calc} | / \Sigma_{hkl} F_{obs}$ where all reflections belong to a test set of 5 %.

cate a feature that is typical of a leucine binding pocket [29] (**Figure 2B**). There is another very important feature of MsPth structure that pertains to the flexibility of the segment Gly138 - Val150. An examination of the values of B - factors of the residues of this segment shows that the B - values increase abruptly at residue, Gly138 but these drop gradually after residue, Pro146 to the optimum level at residue, Val150. The highest values are observed for residues, Gly142 and Arg143 both of which are part of the tight type II' β-turn conformation and interestingly, these two residues are located at the centre of the segment Gly138 - Val150 indicating domain-like movement of the segment with respect to the rest of the body of the molecule.

Structural comparisons with MtPth and EcPth

The sequence of MsPth consists of 191 amino acid residues and the positions of protein atoms from all the 191 residues were determined unambiguously using X-ray crystallographic method. The sequence of amino acid residues of MtPth also contains 191 amino acid residues but the structure determination could reveal the positions of atoms from only 179 residues [14]. The sequence of EcPth has 193 residues (**Figure 3**) and the positions of all the atoms from 193 residues were reported. The superimposition of C^a atoms of 179 residues of MsPth on those of MtPth shows an r.m.s. deviation of 1.1 Å whereas the r.m.s. shift for all the atoms was found to be 2.6 Å. The r.m.s shift when C^a atoms of 191 residues of MsPth and EcPth were superimposed was found to be 2.2 Å. It means that the overall structure of EcPth is considerably different from that of MsPth and hence only a limited comparison will be made with it. The regions of the MsPth structure that deviate prominently from the corresponding segments of MtPth and EcPth include residues 1 - 5 (N-terminus), 34 - 62 (loop α1 - β2, β-strands, β2, β3 and β4), 138 - 150 (loop β7 - α4 and α-helix, α4) and the segment 180 - 191 (C-terminal region including α-helix, α6). It may be noted here that the C-terminal stretch of residues, 180 - 191 was not observed in MtPth [14] while its N-terminal residues, 1 - 5 were poorly defined. In this regard, it is important to note that in MsPth, Gln89 stabilizes the N-terminal segment effectively by forming two hydrogen bonds with the backbone atoms of Glu3 and Pro4 (Gln89 N^{e2} - - - O Glu3 = 3.1 Å and Gln89 N^{e2} - - - O Pro4 = 2.9 Å). The residue corresponding to Gln89 is Asn89 in MtPth and forms only one weak hydrogen bond with the side chain atom of Glu3 (Asn89 N^{d2} - - - O^{e1} Glu3 = 3.3 Å). On the other hand, the chain of EcPth is shorter by one residue at the N-terminus and appears to be optimally well

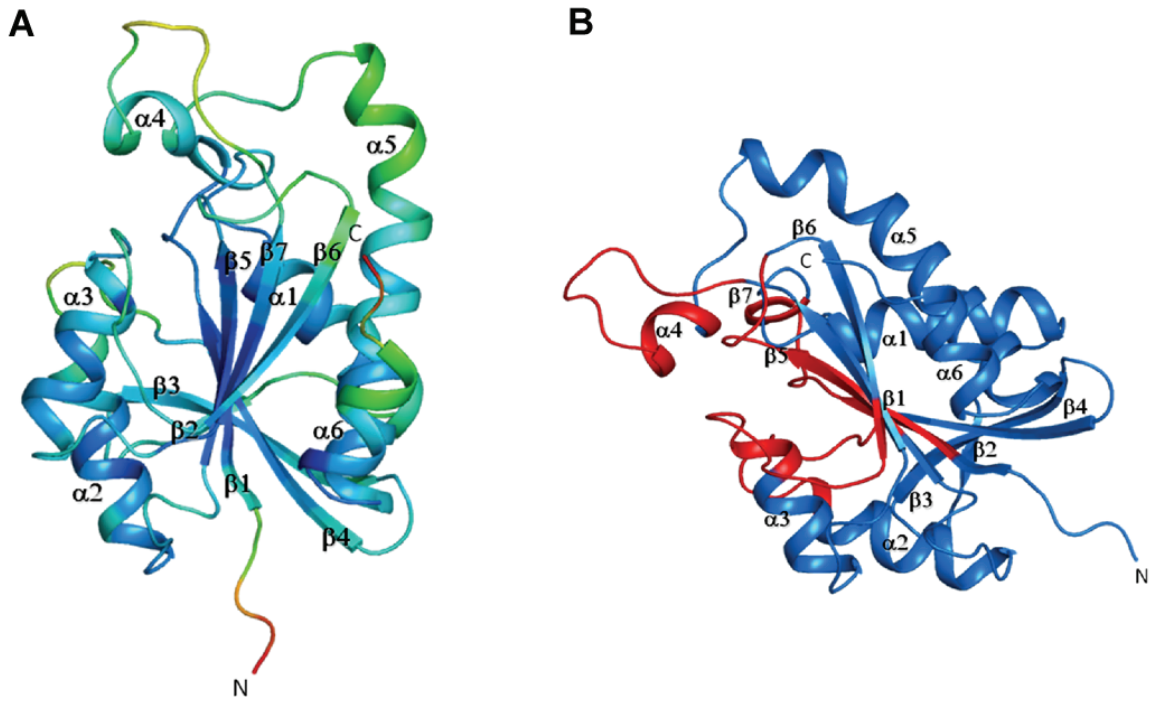

Figure 1. Structure of MsPth depicted as ribbons: (A) a topology with twisted β-sheet at the center showing color coded B-factors with B-values of 50-75 Å^2 (red), 40-50 Å (green), 20-30 Å^2 (aquamarine) and 10-20 Å^2 (blue) (B) Ribbon diagram of MsPth with secondary structure elements labeled as β-strands, β1 – β7 and α-helices as α1 – α6. The substrate binding site is indicated in red colour. Figure was drawn using Pymol [28].

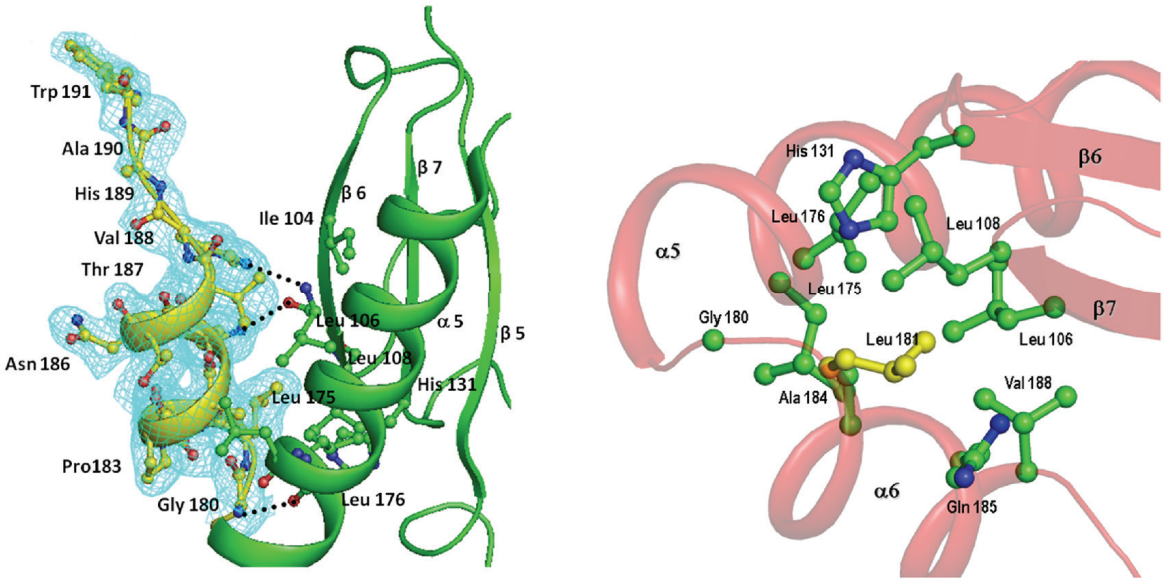

Figure 2. (A) A view of the ordered C-terminal segment (Gly180 - Trp191) (yellow) with respect to neighboring segments in the protein (green). The omit electron density for the C-terminal segment at 2s cut off is also indicated. The hydrogen bonds involving C-terminal residues are indicated by dotted lines. A number of hydrophobic residues are also shown in the proximity of Leu181. (B) The position of Leu181 in the hydrophobic leucine binding pocket is shown.

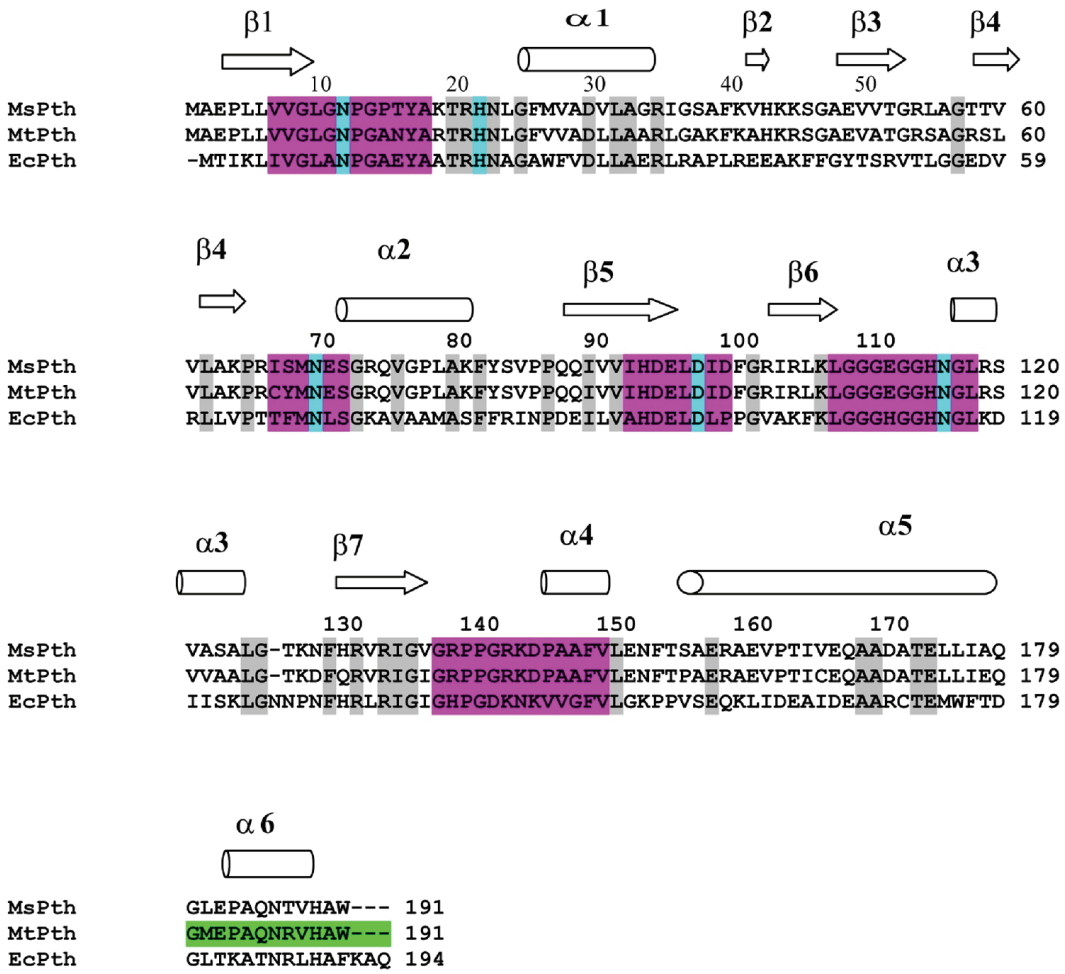

Figure 3. Multiple sequence alignment of peptidyl - tRNA hydrolses (Pth) from *Mycobacterium smegmatis* (MsPth), *Escherichia coli* (EcPth) and *Mycobacterium tuberculosis* (MtPth) is performed using ClustalW [27]. The first column shows the protein identifier. The identical residues are colored in grey, substrate - binding active site residues are shown in cyan. The segments associated with substrate - binding cleft are shaded in pink. The secondary structure elements of Pth protein are schematized above the sequence with β-strands represented as arrows and α-helices as cylinders. The C-terminal segment (180 - 191) indicated in green is absent in the structure of MtPth.

integrated with the rest of the protein through intramolecular contacts. The C-terminal segment in MsPth is well defined with a number of intramolecular contacts involving the C-terminal residues. The prominent interactions include at least three hydrogen bonds and several van der Waal's contacts. The C-terminal residues, His189, Gln185 and Gly180 form hydrogen bonds with other parts of the protein molecule while the side chain of Leu181 is held firmly in a hydrophobic pocket which is formed with residues Leu106, Leu108, His131, Leu 175, Leu176, Ala184, Glu185. In contrast, the twelve C-terminal residues (180 - 191) of MtPth were not observed which were presumably disordered due to lack of interactions particularly those involving Leu181 as it is replaced by Met181 in MtPth which may not be optimally accommodated in the hydrophobic pocket. Furthermore, the hydrophobic pocket is also not formed properly due to the replacements of Leu108 and His131 by Ile108 and Gln131 respectively. As a result of a relatively poor packing, the conformation of the C-terminal segment in MtPth might have been considerably disordered and hence it could not be observed in the crystal structure of MtPth [14]. In contrast, the structure of C-terminal region in EcPth is substantially different partly because the corresponding hydrophobic pocket is formed slightly

differently with three aromatic residues, Phe106, His131 and Trp176. Also, since the C-terminal tripeptide, Lys191 - Ala192 - Glu193 is inserted into the substrate - binding cleft of the neighboring molecule during molecular packing in the crystals, thereby stabilizing the C-terminal segment. In this context, it is important to note the presence of three extra amino acid residues at the C-terminus in EcPth. This elongation of the C-terminal part may be essential for the interaction with the substrate - binding cleft of another molecule leading to stabilization of the C-terminal residues in EcPth. However, this tendency of blocking the substrate - binding site of another molecule is also suggestive of a self inhibitory action in EcPth although a similar molecular association has not been observed so far in solution indicating a low binding affinity.

In order to understand the features of the region which is believed to be involved in peptide and tRNA binding, it is important to examine the roles of protein segments, Gly9 - Ala18, Ile67 - Ser 72, Ile93 - Asp100, Leu108 - Leu118, and Gly136 - Asn153 which are part of the substrate - binding cleft. In EcPth residues, Asn12, Tyr17, Asn70, and Asn116 (MsPth numbering) were observed forming intermolecular interactions with the C-terminal segment of the neighbouring molecule in the crystal packing. This was used as the basis for having identified the cleft as a potential binding site for the peptide part of the substrate, peptidyl - tRNA although similar molecular packings have not been observed in the crystal structures of MtPth [14] and MsPth (present structure). The lack of such an interaction in the present structure may apparently be due to the reason that the C-terminal segment is tightly held with the rest of the protein and may not be easily detachable to interact with the residues of the substrate - binding cleft of the neighboring molecule although it may provide an essential contribution to interact with the tRNA part of the peptidyl-tRNA when the substrate peptidyl-tRNA is introduced. In the case of MtPth, the C-terminal segment appears to be highly disordered and thus it is unable to interact with the substrate - binding cleft of the neighboring molecule in a similar way as observed in EcPth. Indeed, it may require stronger attractions to be able to participate in the intermolecular interactions as might be provided by the substrate molecule, peptidyl - tRNA.

Discussion

One of the most striking features of the peptidyl -tRNA hydrolase structures pertains to the conformation of the loop Gly138 - Val150 (**Figure 4A**). It is observed that the segment, Gly138 - Val150 adopts different conformations in the structures of MsPth, MtPth and EcPth indicating the highly flexible states of the loop (Gly138 - Val150) which may be required for the substrate recognition by these proteins to accommodate a variety of peptide moieties of peptidyl - tRNA hydrolases. In the case of EcPth, the widened cleft, due to the moving away of the loop Gly138 - Val150, presumably due to the bound peptide, is closed by the positioning of Lys142 after the binding had occurred which may possibly interact with tRNA moiety after the peptide is anchored in the cleft while in the case of MtPth due to different positioning of the flexible loop, the corresponding residue Arg143 is pointing in an almost opposite direction to that of Lys142 of EcPth. In contrast, in the present structure of MsPth, the Gly138 - Val150 loop is oriented differently with the corresponding Arg143 oriented at about 90° from the directions of both Lys142 in EcPth and Arg143 in MtPth (**Figure 4B**). The conformation of the loop Gly138 - Val150 is apparently guided by a few key interactions involving this loop (**Figure 5A**). In MtPth, Asp98 forms a salt bridge with Arg139 (**Figure 5B**) as a result of which the side chain of Arg139 turns towards the backbone causing narrowing of the loop at the site of Arg143 with a unique positioning of Lys144 (**Figure 6**). In this case, Arg21 forms a salt bridge with Glu158. It is completely different in MsPth where Arg139 does not interact with Asp98. In contrast, a strong salt bridge is observed between Lys144 and Glu152 which broadens the internal space of the loop pushing Arg143 outwardly at an angle of 90° from the base of the backbone (**Figure 5A**). In MsPth, Arg21 provides the loop stabilizing interactions by simultaneously interacting with Phe149 O and Glu 158 $O^{\delta 2}$. The environment in EcPth is very different where an external salt bridge involving Asp141 and Lys144 guides the final conformation of the loop and the residue corresponding to Lys144 in MsPth is Asn143 in EcPth which is oriented in an altogether different direction. However, Arg19 interacts with both Phe148 and Glu157. It may also be noted here that the residue corresponding to Asp141 of EcPth is Gly142 in both MtPth and MsPth. These interactions indi-

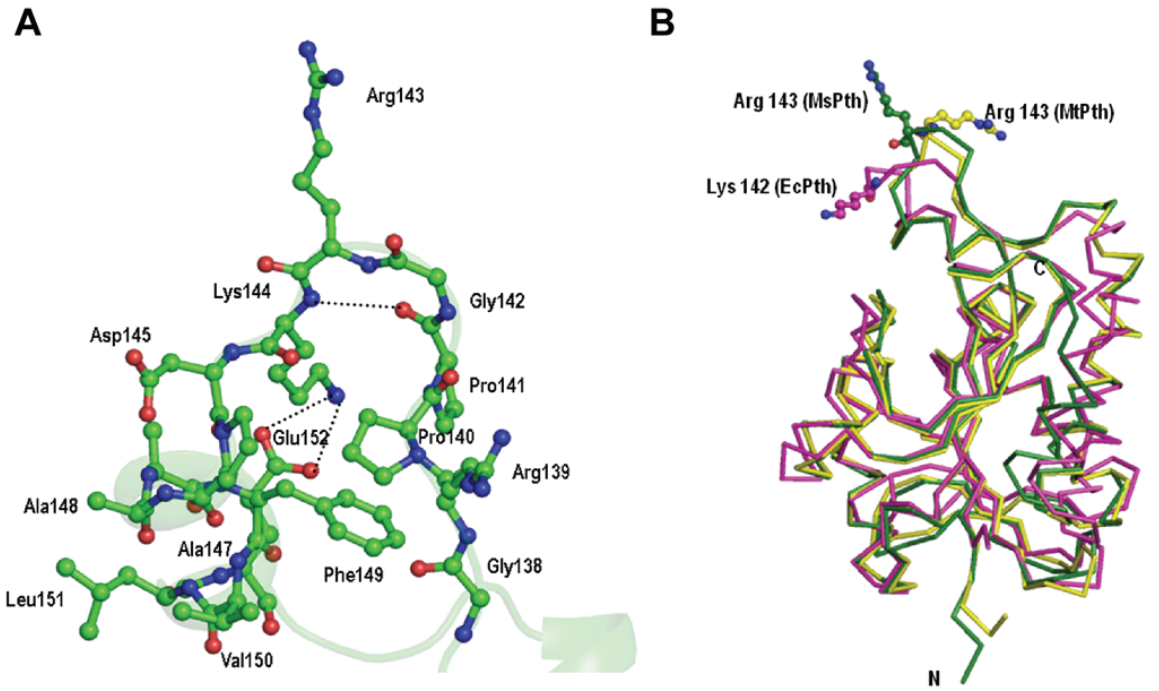

Figure 4. (A) The mobile segment Gly138 - Val150 showing the position of Arg143 and salt bridge formed between Lys144 and Glu152 as unique features of the structure of MsPth. The dotted lines indicate hydrogen bonds and salt bridges. (B) The superimpositions of C^{α} traces of MsPth (green), MtPth (yellow) and EcPth (pink). The side chains of Arg143 of MsPth (green), MtPth (yellow) and the corresponding residue Asn142 from EcPth (pink) are also shown.

cate that the movements of the loop Gly138 - Val150 are differently regulated in these proteins suggesting potentially important differences in the modes and rates of substrate bindings.

Yet, another important feature in these structures concerns with the formation of a β-reverse turn between β-strand β6 (103 - 108) and α-helix α3 (116 - 125) which determines the shape and position of one of the sides at the opening of the gate to the substrate - binding cleft. The supposedly flexible tetrapeptide Glu112 - Gly113 - Gly114 - His115 (**Figure 6**) from one side of the cleft adopts a rather tight type II' β-turn conformation with a characteristic intra - turn hydrogen bond, His115 N - - - O Glu112 = 3.1 Å. The distance between Glu112 C^{α} and Asn116 C^{α} is 8.1 Å. The corresponding tetrapeptides in MtPth and EcPth form distorted type I' β-turn conformations with N_{i+3} - - - O_i hydrogen bonds with distances of 3.0 Å and 3.1 Å respectively. The distances between Glu112 C^{α} and Asn116 C^{α} in MtPth and EcPth were found to be 7.7 Å and 7.1 Å respectively indicating a more compact shape of the turn in EcPth and the least tightness in MsPth. It may be attributed to a strong interaction between Gly113 O and the side chain of Arg119 (Gly113 O - - - NH1 Arg119 = 3.3 Å and Gly113 O - - - NH2 Arg119 = 2.9 Å) (**Figure 6A**). The similar interactions are absent in both MtPth and EcPth (**Figures 6B** and **6C**) indicating that the conformation of Gly113 (Φ = 57.2° and Ψ = -134.9°) is different from MsPth than those in MtPth (Φ = 63.3° and Ψ = 20.4°) and EcPth (Φ = 57.7° and Ψ = 27.2°). As a result, the distance between Asp98 $O^{\delta 2}$ and Gly113 C^{α} in the unliganded state is 4.5 Å in MsPth whereas the corresponding value in MtPth is of the order of 3.1 Å - 3.4 Å. As a consequence, the width of the cleft at Asp98 $O^{\delta 2}$ and Gly113 C^{α} is different in the resting states of MsPth and MtPth and this may show different behavior on induction by substrates peptidyl-tRNAs resulting in the different mode of binding and different rate of catalysis. The corresponding distance in the liganded EcPth is 6.7 Å. Yet another relevant distance indicator that reflects the variable position of the flexible loop Gly138 - Val150 is

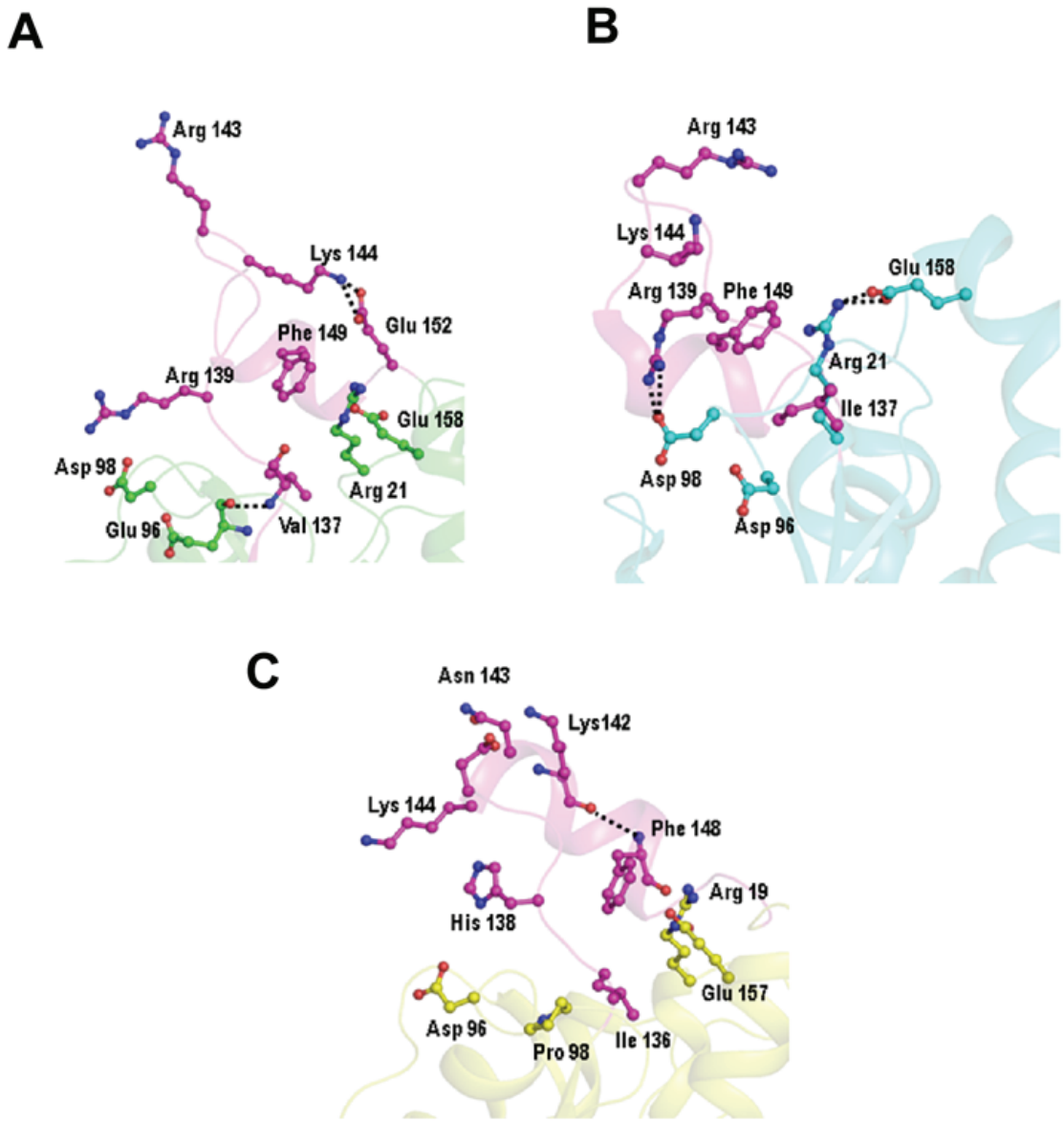

Figure 5. The roles of Arg139 and Arg21 in stabilizing the conformation of the loop Gly138 - Val150 in (A) MsPth: Arg139 does not interact with Asp98 while Arg21 forms a hydrogen bond with Phe1490. Glu158 forms a salt bridge with Lys144; (B) MtPth: Arg139 forms a salt bridge with Asp98 while Arg21 interacts with Glu158. Lys144 does not interact intramolecularly and (C) EcPth: The residue corresponding to Arg139 is His138 which is not involved in the intramolecular interactions. The residue corresponding to Arg21 is Arg19 which is not involved in interactions. Lys142 (corresponding to Arg143 in MsPth) hangs outwardly from the molecule.

between Ala147 C^{α} - Gly114 C^{α} which is 7.8 Å in MsPth while the corresponding distances in MtPth and EcPth are 9.5 Å and 11.8 Å respectively. These values clearly indicate that the flexibility and mobility of the loop Gly138 - Val150 in peptidyl-tRNA hydrolases are not identical in these three proteins which may get adjusted upon the binding of substrates according to the sizes of their peptide moieties.

From the structural model of EcPth as well as from the mutational studies, it has been indicated that the residues Asn116, His22 and Asp95 may be involved in catalysis. The struc-

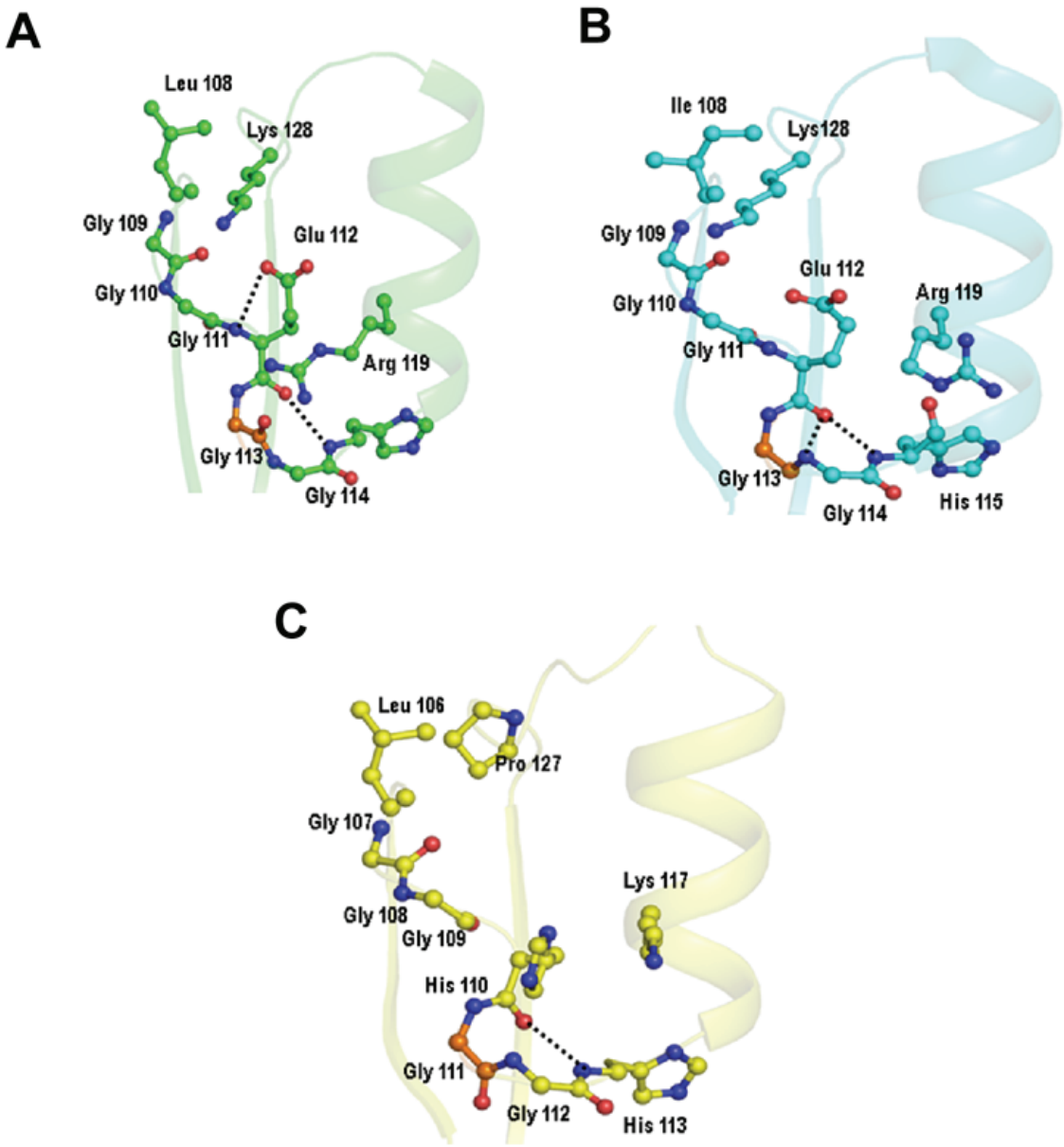

Figure 6. The conformation and stability of one of the sides of the substrate - binding cleft, residues (108 - 118): (A) MsPth, (B) MtPth and (C) EcPth. The dotted lines indicate hydrogen bonds. Particularly noteworthy is the position of Gly113 O (orange) in the three structures. In MsPth, it differes from those in MtPth and EcPth.

ture of MsPth revealed that Asn116 $N^{\delta 2}$ forms a hydrogen bond with His22$N^{\varepsilon 2}$ (3.0 Å) while His22$N^{\delta 1}$ is hydrogen bonded to Asp95$O^{\delta 2}$ (2.8 Å) (**Figure 7**). This arrangement appears to be stereochemically favorable for the enzymatic activity. It is noteworthy that a series of positively charged residues and other ionic residues make a favorable site for a potential interaction with tRNA moiety.

Concluding remarks

The peptidyl - tRNA hydrolase from *Mycobacterium smegmatis* is a single domain 21k Da protein without a salt bridge. It hydrolyzes peptidyl-tRNAs which are a mixture of substrates consisting of peptide moieties of variable lengths. The protein chain adopts an α/β fold with a twisted β-sheet in the centre which is sur-

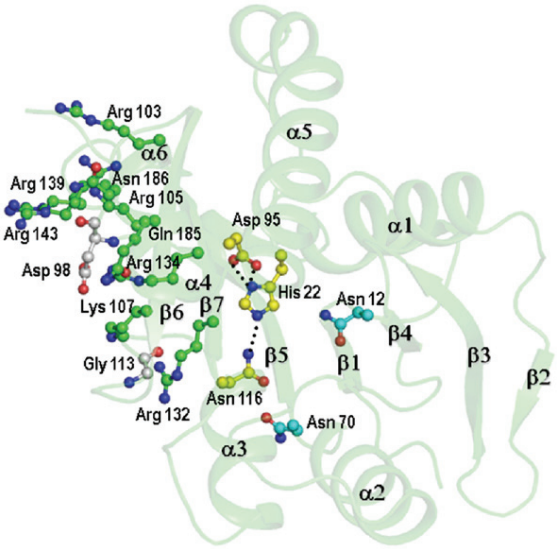

Figure 7. Showing residues that interact with the substrate molecule including those involved in the catalysis. The dotted lines indicate hydrogen bonds.

rounded from two sides by α-helices. The main features of this protein are the formation of a substrate - binding cleft consisting of protein segments Gly9 - Ala18, Ile67 - Ser72, Ile93 - Asp100, Leu108 - Leu118 and Gly136 - Asn153, a domain-like mobile segment (residues 138 - 150), a flexible C-terminal segment (180 - 191), a slightly rigid side of the cleft (residues 109 - 118) and the substrate - binding residues Asn12, His22, Asn70, Asp95 and Asn116 which are conserved in Pth from various species. The observed structures of Pth from three bacterial species, *Mycobacterium smegmatis* (MsPth), *Mycobacterium tuberculosis* (MtPth) and *Escherichia coli* (EcPth) indicate different states of flexibility for the loops 109 - 118, 138 - 150 and the C-terminal segment, 180 - 191. The flexible nature of the protein appears to be essential to accommodate the different sizes of peptide moieties and the negatively charged phosphate group of tRNA. The observed differences in the flexible states of three bacterial species caused primarily by different intra - molecular interactions suggest that the substrate affinities, mode of binding and rates of catalysis may differ in these proteins. In view of a variety of bacterial infections and the growing incidences of bacterial resistance to antibiotics, it is important to produce common structural details for developing universal drugs to control bacterial infections. In this regard, the structure determination of MsPth has provided a variety of mechanistic aspects of intramolecular interactions related to enzyme dynamics and ligand design.

Protein data bank accession codes

The atomic coordinates and the structure factors have been deposited in the RCSB Protein Data Bank with the accession code 3KJ2.

Acknowledgements

The authors acknowledge financial support from the Department of Science and Technology, New Delhi. AK thanks University of Grant Commission, New Delhi for the award of fellowship to him. TPS thanks Department of Biotechnology, New Delhi for the award of Distinguished Biotechnology Research Fellowship.

Address correspondence to: Dr. Singh TP, Department of Biophysics, All India Institute of Medical Sciences, Ansari Nagar, New Delhi - 110 029, India Tel: +91-11-2658-8931; Fax: +91-11-2658-8663; E-mail: tpsingh.aiims@gmail.com

References

[1] Das G, Varshney U. Peptidyl-tRNA hydrolase and its critical role in protein biosynthesis. Microbiology 2006; 152: 2191-2195.

[2] Singh NS, Varshney U. A physiological connection between tmRNA and peptidyl-tRNA hydrolase functions in *Escherchia coli*. Nucleic Acids Res 2004; 32: 6028-6037.

[3] Heurgue-Hamard V, Karimi R, Mora L, MacDougall J, Leboeuf C and Grentzmann G. Ribosome release factor RF4 and termination factor RF3 are involved in dissociation of peptidyl-tRNA from the ribosome. EMBO J 1998; 17: 808-816.

[4] Karimi R, Pavlov MY, Heurgue-Hamard V, Buckingham RH and Ehrenberg M. Initiation factors IF1 and IF2 synergistically remove peptidyl-tRNAs with short polypeptides from the P-site of translating *Escherichia coli* ribosomes. J Mol Biol 1998; 281: 241-252.

[5] Guarneros G. The rate of peptidyl-tRNA dissociation from the ribosome during minigene expression depends on the nature of the last decoding interaction. J Biol Chem 2003; 278: 26065-26070.

[6] Cuzin F, Kretchmer N, Greenberg RE, Hurwitz R and Chapeville F. Enzymatic hydrolysis of N-substituted aminoacyl tRNA. Proc Natl Acad Sci USA 1967; 58: 2079-2086.

[7] Menninger JR. Peptidyl transfer RNA dissociates during protein synthesis from ribosomes

of *Escherchia coli*. J Biol Chem 1976; 251: 3392-3398.
[8] Menninger JR. Accumulation of peptidyl tRNA is lethal to *Escherichia coli*. J Bacteriol 1979; 137: 694-696.
[9] Kossel H, RajBhandary UL. Studies on polynucleotides LXXXVI. Enzymatic hydrolysis of N-aminoacyl-transfer RNA. J Mol Biol 1968; 273: 389-401.
[10] García-Villegas MR, De La Vega FM, Galindo JM, Segura M, Buckingham RH and Guarneros G. Peptidyl-tRNA hydrolase is involved in inhibition of host protein synthesis. EMBO J 1991; 10: 3549-3555.
[11] Rosas-Sandoval G, Ambrogelly A, Rinehart J, Wei D, Cruz-Vera LR and Graham DE. Orthologs of a novel archaeal and of the bacterial peptidyl - tRNA hydrolase are nonessential in yeast. Proc Natl Acad Sci USA 2002; 99: 16707-16712.
[12] Bonin PD, Choi GH, Trepod CM, Mott JE, Lyle SB, Cialdella JI, Sarver RW, Marshall VP and Erickson LA. Expression, purification and characterization of peptidyl-tRNA hydrolase from *Staphylococcus aureus*. Protein Expr Purif 2002; 24: 123-130.
[13] Schmitt E, Mechulam Y, Fromant M, Plateau P and Blanquet S. Crystal structure at 1.2 Å resolution and active site mapping of *Escherichia coli* peptidyl-tRNA hydrolase. EMBO J 1997; 16: 4760-4769.
[14] Selvaraj M, Roy S, Singh NS, Sangeetha R, Varshney U and Vijayan M. Structural plasticity and enzyme action: crystal structures of Mycobacterium tuberculosis peptidyl-tRNA hydrolase. J Mol Biol 2007; 372: 186-193.
[15] Bal NC, Agarwal H, Meher AK and Arora A. Characterization of Peptidyl-tRNA hydrolase encoded by open reading frame Rv1014c of *Mycobacterium tuberculosis* H37Rv. Biol Chem 2007; 388: 467-479.
[16] Fromant M, Schmitt E, Mechulam Y, Lazennec C, Plateau P and Blanquet S. Crystal structure at 1.8 Å resolution and identification of active site residues of *Sulfolobus solfataricus* peptidyl-tRNA hydrolase. Biochemistry 2005; 44: 4294-4301.
[17] De Pereda JM, Waas WF, Jan Y, Ruoslahti E, Schimmel P and Pascual J. Crystal structure of a human peptidyl-tRNA hydrolase reveals a new fold and suggests basis for a bifunctional activity. J Biol Chem 2004: 279: 8111-8115.
[18] Shimizu C, Kuroishi M, Sugahara and Kunishima N. Structure of peptidyl-tRNA hydrolase 2 from *Pyrococcus horikoshii* OT3: insight into the functional role of its dimeric state. Acta Crystallogr 2008; D64: 444-453.
[19] Kremer L, Baulard A, Estaquier J, Poulain-Godefroy O and Locht C. Green fluoroscent protein as new expression marker in mycobacteria. Mol Microl 1995; 17: 913-922.
[20] Vagin A, Taplyakov A. MOLREP: an automated program for molecular replacement. J Appl Crystallogr 1997; 30: 1022-1025.
[21] Brunger AT, Adams PD, Clore GM, DeLano WL, Gros P, Grosse-Kunstleve RW, Jiang JS, Kuszewski J, Nilges M, Pannu NS, Read RJ, Ric LM, Simonson T and Warren GL. Crystallography and NMR System: a new software suite for macromolecular structure determination. Acta Crystallogr 1998; D54: 905-921.
[22] Emsley P, Cowtan K. Coot: model-building tools for molecular graphics. Acta Crystallogr 2004; D60: 2126-2132.
[23] Jones TA, Zou JY, Cowan SW and Kjeldgaard M. Improved methods for building protein models in electron density maps and the location of errors in these models. Acta Crystallogr 1991; A47: 110-119.
[24] Davis IW, Leaver-Fray A, Chen VB, Block JN, Kapral GJ, Wang X, Murray LW, Arenddall WB, Snoeyink J, Richardson JS and Richardson DC. MolProbity: all-atom contacts and structure validation for proteins and nucleic acids. Nucleic Acids Res 2007; 35: W375-W383.
[25] Laskowski RA, MacArthur MW, Moss DS and Thornton JM. PROCHECK: a program to check stereo chemical quality of protein structures. J Appl Crystallogr 1993; 26: 283-291.
[26] Ramachandran GN, Sasisekaran V. Conformation of polypeptides and proteins. Adv Protein Chem 1968; 23: 283-438.
[27] Chenna, Ramu, Sugawara, Koike H, Lopez T, Gibson R, Higgins HJ, Desmond G and Thompson JD. Multiple sequence alignment with clustal sequence of programs. Nucleic Acids Res 2003; 31: 3497-3500.
[28] DeLano WL. The PyMol molecular Graphics System, DeLano Scientific, San Carlos CA. 2002; http://www.pymol.org.
[29] Lo KP, Murphy ME, Guillemette JG, Smith M and Brayer GD. Replacements in a conserved leucine cluster in the hydrophobic heme pocket of cytochrome c. Prot Sci 1995; 4: 198 -208.